Rainbow effect in axial ion channeling

H. F. Krause, S. Datz, P. F. Dittner, J. Gomez del Campo, P. D. Miller, C. D. Moak, N. Nešković,* and P. L. Pepmiller
Oak Ridge National Laboratory, Oak Ridge, Tennessee 37831
(Received 28 October 1985)

We have studied the angular scattering distributions produced in axial channeling when incident protons (7 MeV) are well aligned to the axial direction of a thin silicon crystal (1400 Å). Measured angular distributions obtained in the ⟨100⟩ and ⟨110⟩ directions using a two-dimensional (2D) position-sensitive detector (resolution $\lesssim 0.015°$) have been interpreted by comparison with Monte Carlo trajectory calculations for these channels in the momentum approximation. The measured angular distributions show structures at certain off-axis angles which are in good agreement with the calculations. The general shape and structure in the angular contour map for a given channel have been shown to be a consequence of extrema in the 2D classical deflection functions for the two Cartesian scattering angles in the detection plane. The occurrence of the extrema in a very thin crystal (i.e., a rainbow effect in axial channeling) is a consequence of the channeling geometry when atomic strings surrounding the axial channel interact with the projectile simultaneously.

I. INTRODUCTION

Considerable effort has been directed toward a detailed understanding of the transmitted angular distribution for ions channeled along the axial directions of single crystals.[1] It is well known that when the projectile energy is low enough and/or when the crystal is thick enough to cause significant multiple-scattering effects, the transmitted beam becomes concentrated along the chosen axis with lower intensity arms extending radially outward along the principal planar directions. Under these conditions, a characteristic "star pattern" is observed and is useful in determining the crystal orientation in channeling experiments.

For a very thin crystal with a tightly collimated projectile beam, the pattern of transmitted particles is known to be more complex and not so well understood. Previous axial-channeling studies performed under these conditions suggest that the transmitted patterns depend on the fine details of the trajectories inside the crystal.[1,2] These qualitative observations have resulted primarily from visual and photographic studies. Since these experiments did not produce angular distribution contour maps that are linear in intensity, the investigators were not able to explain their results quantitatively. Quantitative experimental and theoretical studies in axial channeling were carried out by Rosner *et al.*, who sought to understand the "doughnut" angular distribution produced when the projectile direction deviates from the crystal's axial direction.[3] Heretofore, however, no angular distributions exiting very thin crystals have been quantified and reported where the projectile and the axial direction are aligned.

Our interest in axial-channeling angular distributions in very thin crystals arose from a desire to explain velocity-dependent charge fractions produced in the resonant-coherent excitation (RCE) process.[4] For example, in the case of channeled one-electron ions, the $1s \rightarrow 2p$ energy spacing is a function of its position in the potential gradient between the atomic rows, so detailed trajectories of the projectile ions must be considered in a calculation of RCE effects. The need for an efficient and accurate computational algorithm stimulated a theoretical investigation of projectile angular deflections in very thin crystals.[5] This investigation[5,6] resulted in the prediction of flux enhancements that could occur at certain exiting angles due to a rainbow effect when the projectile and crystal axes are aligned (in analogy to the peaking of light flux scattered from water droplets at certain angles in optical rainbows). Rainbow scattering has been observed at low energies (thermal to 100 eV) in atom-atom scattering,[7] in atom-surface scattering[8] and at high energies in nuclear scattering of heavy nuclei.[9] The rainbow effect was even noted during the early days of channeling[10] in a blocking context when Oen interpreted the anisotropy of α particles emitted from a monocrystalline W tungsten single crystal.[10] However, blocking studies offered no hint of our findings, and the rainbow effect in transmitted axial-channeling angular distributions has remained unexplored until the present. In this work we have studied 7-MeV protons channeled along the ⟨100⟩ and ⟨110⟩ axes of a very thin silicon single crystal using a 2D position-sensitive detector to measure the transmitted angular distribution and compare these results with theoretical calculations based on the model of Nešković.[6]

II. THEORY

The origin of the rainbow in scattering processes is an extremum in the classical deflection function that gives rise to an infinite differential cross section at certain scattering angles. In order to show that the rainbow can occur in axial channeling, we will examine the deflection function for the case of an axially channeled projectile and show where $d\theta/d\mathbf{b}$ has extrema. To obtain the deflection function, we consider an ion incident on an axial channel with initial impact parameter determined by the

Cartesian coordinates $\mathbf{b}=(x,y)$ (measured from channel center) and moving parallel to the direction of atomic strings defining the channel, along the z axis. We shall assume that the transverse momentum imparted to the projectile, $\mathbf{P}_\perp=(p_x,p_y)$, is very small compared to the incident projectile momentum, $\mathbf{P}_0(P_0=p_z)$, and that the crystal is sufficiently thin so $|\mathbf{P}|/P_0$ is less than the geometrical width-to-length ratio of the channel. In this case the ion trajectory may be approximated in the small-angle limit by a straight line. Under these conditions, the transverse momentum can be calculated via Eq. (1), starting from an assumed force center with potential $U_i(x,y,z)$,

$$\begin{aligned}\mathbf{P}_\perp &= -N\sum_{i=1}^{M}\int_{-\infty}^{\infty}\nabla_\perp U_i(x,y,z)dt \\ &= \frac{Nm_1}{P_0}\sum_{i=1}^{M}\nabla_\perp V_i(x,y)\,, \\ V_i(x,y) &= \int_{-\infty}^{\infty}U_i(x,y,z)dz\,.\end{aligned} \tag{1}$$

Equation (1) is a simple extension to axial channeling of the harmonic scattering problem discussed by Demkov,[11] where the net transverse momentum is the vector sum of the transverse momentum contributed by each atomic string surrounding the channel (i.e., the ith string), M is equal to the number of strings that contribute significantly, here taken to be equal to the number of strings lying within the third-coordination circle about channel center, N is the number of atoms in one string, and m_1 is equal to the projectile mass. The impact-parameter-dependent deflection function $\theta(x,y)$ is equal to $\mathbf{P}_\perp/P_0$ in the small-angle limit. $V_i(x,y)$ is the average transverse (continuum) potential for the ith atomic string based on a specific interatomic potential, $U_i(x,y,z)$.[12] Here we use the Lindhard continuum potential, which is an approximate Thomas-Fermi potential.[12,13] As noted by Demkov, the effective differential cross section is defined as the Jacobian of the transformation

$$\sigma(p_x,p_y)=2m_1E\sum\left|\frac{\partial(x,y)}{\partial(p_x,p_y)}\right|\,, \tag{2}$$

where the summation is over all the values of the multiply valued function $b(P_\perp)$ and E denotes the projectile energy. The cross section is defined as the ratio of the area elements on the impact-parameter plane and the scattering plane, respectively. Nešković[6] has shown that the Jacobian is unbounded along lines in the scattering plane defined as the rainbow ridge. We shall show that this is true in a complementary fashion by examining the impact parameter dependence of the deflection function.

In order to illustrate the rainbow and show that it is a consequence of geometrical string arrangement, consider the ⟨100⟩ axial channel defined by the four atomic strings shown in Fig. 1(a). Let the two-dimensional (2D) Cartesian scattering angles in the laboratory frame be denoted by (θ_x,θ_y) for the small-angle scattering problem at hand. A projectile entering at the center of the channel $(x=0,y=0)$ will experience a symmetrical repulsion from each string that imparts no net transverse momentum to the projectile in a simultaneous interaction with all strings and therefore the projectile suffers no angular deflection. A particle entering at $(x,\ y=0)$ will experience no deflection in the θ_y direction, but will be increasingly deflected toward negative θ_x as x is increased positively. The deflection function for θ_x, calculated for such a sequence of impact parameters x, is shown in Fig. 1(b). Referring to Fig. 1(b), we see that the deflection angle decreases until it reaches a minimum (a turning point) at the rainbow angle corresponding to $\theta_x=-0.0257°$ (corresponding to an impact parameter of $x=0.98$ a.u.) and then increases until it reaches a turning point (at $+\theta_x$, not shown) in the channel located to the right of that shown in Fig. 1(a).

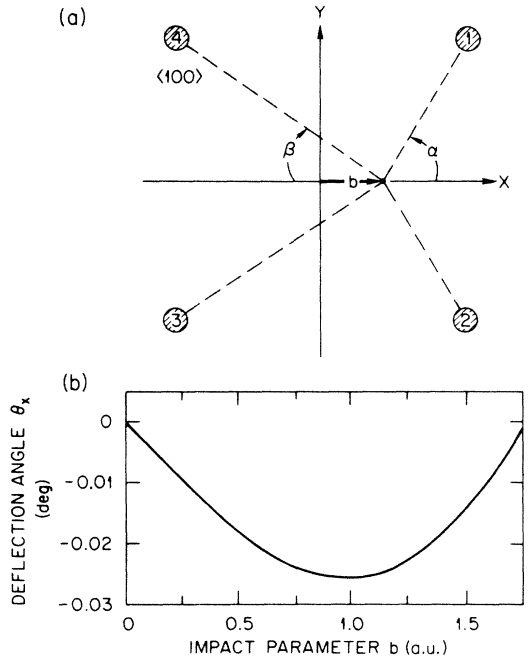

FIG. 1. (a) Atomic string positions for the ⟨100⟩ axis of silicon (3.69 a.u. string spacing in the horizontal and vertical directions). An impact parameter, b, lying along the x axis (and measured from the center of the channel) is shown. (b) Deflection function, $\theta_x(b)$, for a very-thin crystal generated for $y=0$. The deflection function has an extremum which gives rise to the rainbow (see text).

The physical reason for the extremum in the deflection function (i.e., the rainbow) is readily explained on the basis of geometrical considerations. As x increases from the center of the channel, the repulsive force from strings 1 and 2 increases, but the component of these forces in the negative-x direction eventually weakens when the angle denoted by α becomes large. Even though the repulsive interaction with strings 3 and 4 is weakening when the projectile moves closer to strings 1 and 2, the angle denoted by β is decreasing and strings 3 and 4 direct more of the repulsive force in the positive-x direction. Thus we see that the vector sum of monotonically decreasing repulsive forces simultaneously acting on the projectile, in combination with the geometrical location of atomic strings, produces the rainbow effect in axial channeling. Rainbow

scattering in axial channeling is essentially a transverse correlation effect.

The demonstration of an extremum in the 2D deflection function given above, where the impact parameter was varied along a symmetry axis of the string location (i.e., X axis), is relevant to impact-parameter cuts along either the X or Y axis. Extrema or turning points in the 2D deflection function are illustrated more generally in Fig. 2, where each 2D deflection function shown in quadrant III was calculated by increasing the radial impact parameter at a fixed angle above the X axis in quadrant I, starting at the center of the ⟨100⟩ axial channel. Referring to Fig. 2, we observe a different turning point in 2D detection space for each radial cut angle in the impact-parameter plane (i.e., deflection angles in the θ_x or θ_y directions exceeding roughly 0.03° are excluded). We have drawn a dotted line through the turning points for each radial impact parameter cut across the channel to locate the line where the scattering intensity distribution is expected to peak (i.e., a range of impact parameters map to each 2D deflection angle). We shall refer to this line as the rainbow ridge. (See the 60% contours of Fig. 8 for a view of the rainbow ridge in all four quadrants.) Figure 2 only shows the $\theta(\mathbf{b})$ for radial impact-parameter cuts lying relatively close to the X and Y axes where the deflection angles at the extrema do not exceed the angular constraints of the ⟨100⟩ axial-channeling geometry. Exceeding these constraints would cause the scattered projectile to collide with other atomic strings before it leaves the crystal, and these collisions would invalidate our initial assumption of treating the scattering from each string as a lumped ion-string single-scattering event.

The mapping of points in the impact-parameter plane into the 2D Cartesian scattering-angle coordinates of our detector has been discussed assuming that projectile trajectories are unmodified by additional scattering processes. In fact, multiple scattering of the projectile by electrons occurs.[13,14] Using Lindhard's equation (4.3) in Ref. 13 for a rough estimate of the mean-square angular fluctuation of the projectile, $\langle(\delta\Omega_e)^2\rangle$, we obtain the value 7.7×10^{-9} for 7-MeV protons traversing either the ⟨100⟩ or the ⟨110⟩ axial channels of our crystal. This deviation corresponds to a Gaussian width [full width at half maximum (FWHM)] of 0.012° $[2\sqrt{2\ln2}\times\sqrt{\langle(\delta\Omega_e)^2\rangle}]$, and this width is comparable to the angular resolution of our detector. To avoid washing out detailed structure on the "rainbow ridge," one should select the target to minimize $\langle(\delta\Omega_e)^2\rangle$. However, it is possible to show that rainbow scattering occurs in channeling without resolving the ridge.

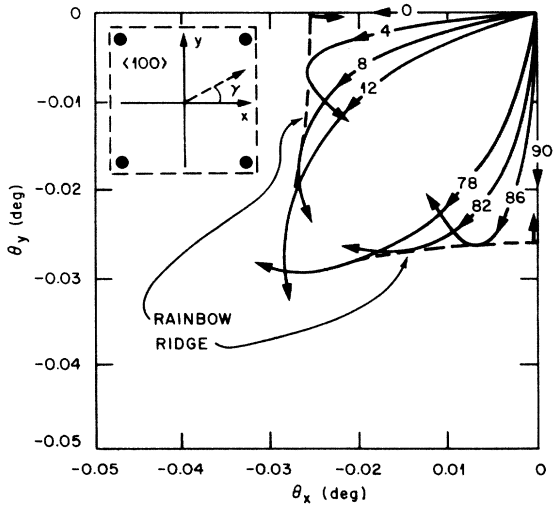

FIG. 2. 2D deflection functions in quadrant III generated by axial impact parameters in quadrant I that are radial cuts through the ⟨100⟩ channel at a fixed angle with respect to the x axis. The impact-parameter angle for each cut is given in degrees. There is a 2D extremum for each cut. The rainbow ridge (dotted-line) is shown passing through the extremum point of each radial cut.

III. EXPERIMENT

In the experimental arrangement shown in Fig. 3, 7-MeV protons produced by the Oak Ridge National Laboratory (ORNL) EN-tandem Van de Graaff accelerator were narrowly collimated (angular divergence $<0.01°$ FWHM) before illuminating a small portion of a silicon single crystal. Axially channeled particles that emerged from the crystal were detected by a 2D position-sensitive proportional counter similar to the one used in Ref. 15. Angular deflections and detector resolution in the horizontal and vertical directions were calibrated absolutely by inserting a carbon foil and a calibration mask between the crystal and the detector, as shown in Fig. 3. The calibration mask consisted of a 2D array of pin holes drilled through an aluminum plate. Phosphors were inserted for aligning the crystal axis to that of the proton beam.

The silicon crystal was cut with the ⟨100⟩ axial direction normal to the surface and was 1400 Å thick. The pathlength was 1980 Å when the crystal was tilted to the ⟨110⟩ axial direction. This thickness corresponds to an atomic string length in the ⟨100⟩ and ⟨110⟩ directions of about 260 and 520 atoms, respectively. The crystal was mounted in a three-axis goniometer that permitted alignment of the axial channel of interest to the beam direction. The illuminated region of the crystal was ~0.5 mm in diameter. While the vacuum conditions surrounding the crystal (1×10^{-6} Torr) did not eliminate the possibility of some carbon deposition on the crystal during the experiments, surface-contaminant buildup probably did not compromise the experimental results at our low-exposure level (about 16 h total exposure at a bombarding current density of order 1000 proton/mm^2 s).

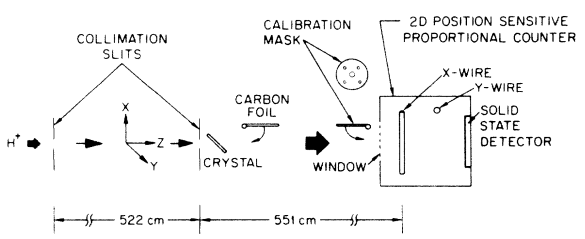

FIG. 3. Sketch of the experimental arrangement. Removable phosphors, situated between the crystal and the detector, that were used during crystal alignment, are not shown.

The 2D position-sensitive gas proportional counter is sketched in Fig. 3. Protons entered the proportional counter through a thin Mylar window (150 $\mu g/cm^2$), traversed the detector volume containing freon-14 at a pressure of 35 Torr, and were detected by a solid-state detector located at the rear of the counter. Secondary electrons originating from the ionization track that drifted to horizontally and vertically oriented anode wires provided the 2D position information. The charge pulse height observed at the ends of each anode wire was digitized for each event signal gated by the solid-state detector. The one-dimensional position was calculated for each wire from the ratio of pulse heights, $q(1)/[q(1)+q(2)]$, where $q(i)$ for $i=1,2$ denotes the charge measured on each end of the wire. The positions for each event were then sorted into a 64 horizontal by 128 vertical 2D array. A Digital Equipment Corporation PDP11/23-based computer-aided measurement and control (CAMAC) system processed the 2D data at a rate up to about 0.5 kHz and an attached Apple III computer provided on-line color contour plotting.

The anode wires, which consisted of a quartz fiber (225 μm diameter) coated with pyrolytic carbon, had a high electrical resistivity. Each anode wire ($+600$ to $+900$ V) was located diametrically opposite a negatively biased planar electrode to produce electric field lines that are predominantly normal to the wire throughout the active length of each detector wire. The horizontal and vertical wires were separated longitudinally by 5 cm for isolation.

The effective detector angular resolution measured in the horizontal and vertical directions was approximately 0.015° and 0.010° (FWHM), respectively, at count rates below 0.5 kHz. Angular resolution in the horizontal direction was limited by the number of horizontal channels available on the data-acquisition system. Detector spatial resolution and the angular size of the illuminated target as viewed from the detector contributed about equally to the overall angular resolution.

IV. RESULTS

A. ⟨110⟩ axial channeling

The experimental 2D angular distribution for 7-MeV protons channeled in the ⟨110⟩ axial direction of silicon is shown in Fig. 4. The data have not been manipulated except for linear interpolation by the contour-plotting routine. Particle-intensity cuts through the distribution at several levels (corresponding to a fraction of the peak count) show that the particle intensity decreases monotonically and very rapidly from that in the undeflected-beam direction. One less intense off-axis peak which lies on the rainbow ridge in the {110} plane at about 0.04° is also observed. From our model calculations we infer that the observed on-axis peak is largely a consequence of our experimental angular resolution. Trajectory calculations suggest that additional off-axis structure lying on the rainbow ridge would be resolvable if the detector angular resolution and angular broadening mechanisms in the crystal combined could be reduced by about a factor of 2. Figure 4 also shows the angular locations of the last atom in each atomic string adjacent to the channel as viewed from the center of the axial channel at a longitudinal location halfway through the crystal. The narrow {100} and wide {111} planar channels that intersect at the ⟨110⟩ axis are also shown. (The {100} and {110} planar channels in silicon are normal to the ⟨110⟩ and ⟨110⟩ axial directions, respectively.)

Evidence of a transverse correlation effect in the angular distribution can be seen without the use of trajectory calculations by comparing contour shapes to the location of the nearest atomic strings. The atomic string placement with respect to the center of the ⟨110⟩ axial channel is different in the {100} and {110} planar directions, and the lowest-level contours of the measured distribution in Fig. 4 reflect the asymmetrical string placement. Major discontinuities in the contours occur in the vicinity of the nearest atomic strings and lines drawn through the discontinuities at the lowest levels appear to point toward the strings. This transverse correlation effect gives rise to a different general shape for the contour map in the case of ⟨100⟩ axial channeling.

The data clearly show that the scattered protons avoid the wide {111} planar channels, preferring instead to be scattered into the narrow {100} planar direction. This preference is a consequence of the rainbow effect. In contrast for a thick crystal, protons multiply scattered at the same energy from the atomic strings surrounding the channel would statistically fill available phase space in planar channels, giving rise to a large number of trajectories in the {111} planar directions and a comparatively

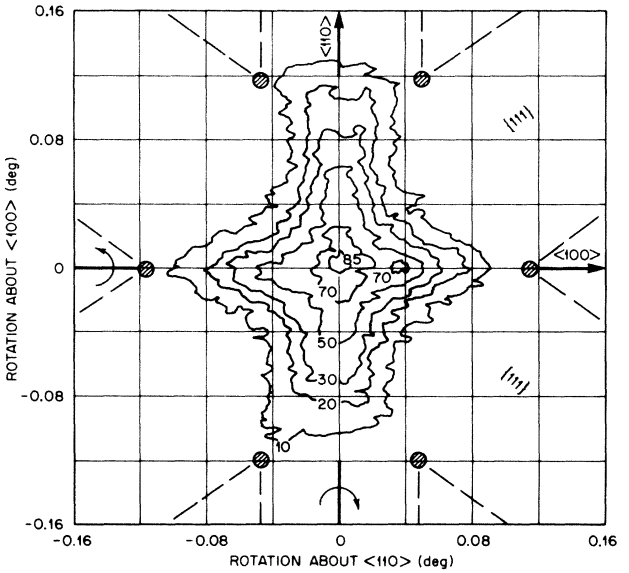

FIG. 4. The experimental angular distribution for 7-MeV protons axially channeled in the ⟨110⟩ direction of silicon (1980-Å thickness, atomic string length 520 atoms). Cuts through the intensity distribution at a fraction of the maximum count (percentages) are plotted as contours at the following levels: 10, 20, 30, 50, 70, 85, 95. Atomic strings lying closest to the center of the channel are shown. The ⟨100⟩ and ⟨110⟩ axial directions are identified. The {100} and {110} planar directions in silicon are normal to the ⟨100⟩ and ⟨110⟩ directions, respectively.

smaller number of trajectories in the {100} planar directions, just opposite to our observations. In essence the rainbow channeling pattern produced by a very thin crystal is best described as an "antichanneling" effect when the intensities in planar directions are compared to those for a thick crystal. We shall also see that these general observations about the transverse correlation effect (i.e., rainbow effect) apply equally well in describing our ⟨100⟩ axial-channeling results.

When we compare the measured angular distribution (Fig. 4) to one obtained in a Monte Carlo trajectory calculation (Fig. 5), details of the 2D angular distribution are predicted for the silicon ⟨110⟩ axis at an energy of 7 MeV. The results in Fig. 5 have been obtained by averaging Monte Carlo angular distributions, obtained with a bin size of 0.002°, over our measured Gaussian angular resolution functions ignoring the angular broadening occurring in the crystal (because its magnitude is not known precisely, and because we expect the magnitude to be impact parameter dependent). In Fig. 5, where contours are drawn at the same levels used in Fig. 4, excellent agreement is shown with respect to general contour shape and overall distribution width at most contour levels. Examining finer detail, two small peaks lying (on the rainbow ridge) in the {110} plane are predicted and one of these peaks was observed at a predicted location. Failure in observing one peak may be the consequence of a slight misalignment of the incident beam and crystal axes in the horizontal plane. Even though the detailed rainbow ridge is not resolved in the experiment, the experimental low-level contours are in agreement with the general contour of the rainbow ridge. This behavior is expected for rainbow scattering because the flux distribution decreases very rapidly for deflection angles greater than the rainbow ridge (where the 2D deflection function extrema are located); therefore particles appearing in the low-level contours are predominantly those scattered into the rainbow and angular broadened by electron multiple scattering. In spite of some differences between the measured and calculated distributions, such as in the horizontal distribution widths moving along the {110} planar direction at several contour levels and smaller differences in the vertical angular width at the 10% level, the observed distribution is well duplicated by the calculation. Evidently, protons at this energy do not undergo significant multiple scattering with atoms along the channel in such a short channel length (1980 Å), and the binary-collision approximations employed for the calculations appear to be appropriate.

B. ⟨100⟩ axial channeling

The measured angular distribution for the ⟨100⟩ axis is shown in Fig. 6. The atomic string positions, positioned as discussed above, are superposed to illustrate the transverse correlation effect. Once again, major discontinuities in the lowest-level contours are observed and lines drawn through the discontinuities appear to point toward the closest atomic strings (compare quadrant III of Fig. 6 with that of Fig. 2). Particle trajectories avoid the wide intersecting planes, which are the {110} planes for this

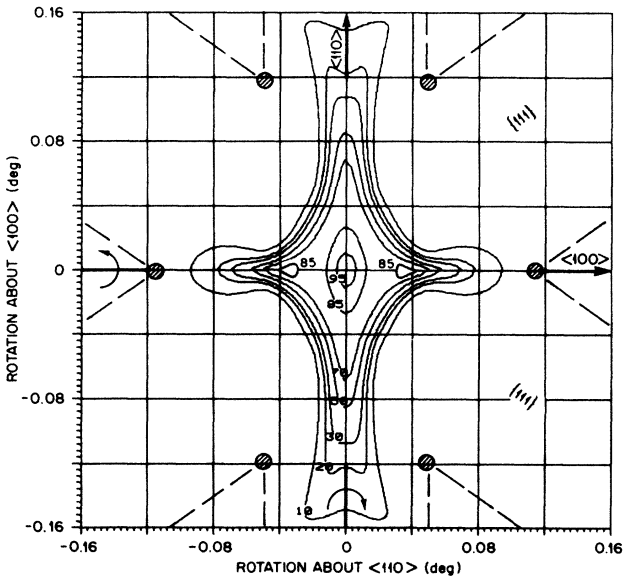

FIG. 5. The calculated angular distribution for 7-MeV protons axially channeled in the ⟨110⟩ direction of silicon. The Monte Carlo calculation assumed a Lindhard potential ($C=4.0$), measured Gaussian angular resolution functions appropriate to the experiment [0.010° vertical; 0.015° horizontal (FWHM)], and the experimental crystal thickness. Cuts through the intensity at a fraction of the maximum intensity (percentage) are plotted as contours at the same levels as Fig. 4. Atomic strings lying closest to the center of the channel are shown. The ⟨100⟩ and ⟨110⟩ axial directions are identified.

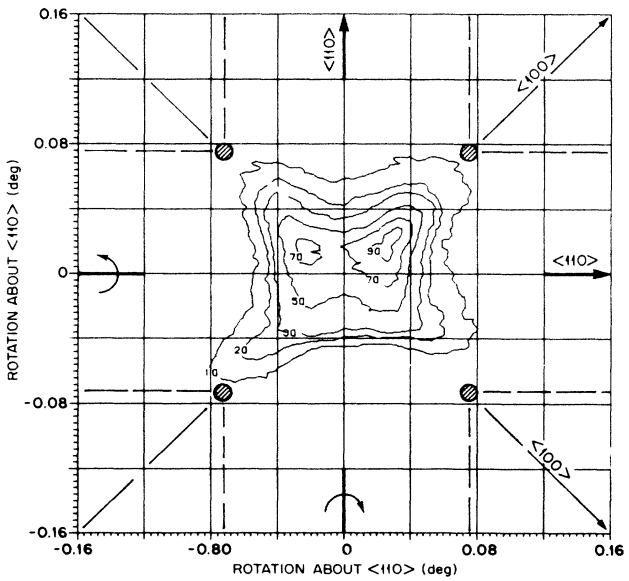

FIG. 6. The experimental angular distribution for 7-MeV protons axially channeled along the ⟨100⟩ direction of silicon where the crystal is 1400 Å thick (atomic string length, 260 atoms). Intensity cuts through the distribution at a fraction of the maximum count (percentage) are plotted as contours at the following levels: 10, 20, 30, 50, 70, 90. Atomic strings lying closest to the center of the channel are shown. The ⟨100⟩ and ⟨110⟩ axial directions are identified.

axial channel. The overall shape of the contours reflects the shape of the rainbow ridge, and this shape is the consequence of the symmetrical location of atomic strings about the ⟨100⟩ axial channel. Some observed asymmetry in the contours suggests that the proton beam was not aligned perfectly to the ⟨100⟩ axis.

Results from our angular averaged Monte Carlo trajectory calculations for the ⟨100⟩ axis are shown in Fig. 7. This calculation used the same thermally averaged Lindhard potential ($C=4.0$) and bin size (0.002°) employed in the ⟨110⟩ calculations. Even after Gaussian averaging, the predicted angular distribution has four off-axis maxima. Each peak lies in the {100} plane, where two branches of the rainbow ridge intersect. The off-axis peaks are better resolved along this axis because fewer trajectories leave the crystal with little or no deflection in the ⟨100⟩ axial direction and the peaks in the ⟨100⟩ distribution are better separated in angle. The highest contour surrounding each peak is not symmetric about the {100} planes in Fig. 7 because of our poorer experimental angular resolution in the horizontal direction; the Monte Carlo results before angular averaging, of course, do not display this asymmetry.

A comparison of Figs. 6 and 7 shows that two of the four predicted peaks have been observed but the observed maxima are not of equal size. A similar situation was noted in our ⟨110⟩ axial measurement. It is likely that the crystal was slightly tilted with respect to the incident proton beam in both the horizontal and the vertical planes. Also, the shape of the lowest level experimental contours (quadrant III) is similar to the rainbow ridge shown in Fig. 2 (dotted line). It again appears that our experimental angular resolution prevented finer details of the rainbow ridge from being resolved. In spite of the small differences that appear in a detailed comparison of the measurements and the calculations, we believe that excellent agreement has been demonstrated for the theoretical assumptions that have been made. We conclude that 7-MeV proton channeling in the ⟨100⟩ axis is also described well by our binary collision approximations for a 1400 Å thick silicon crystal.

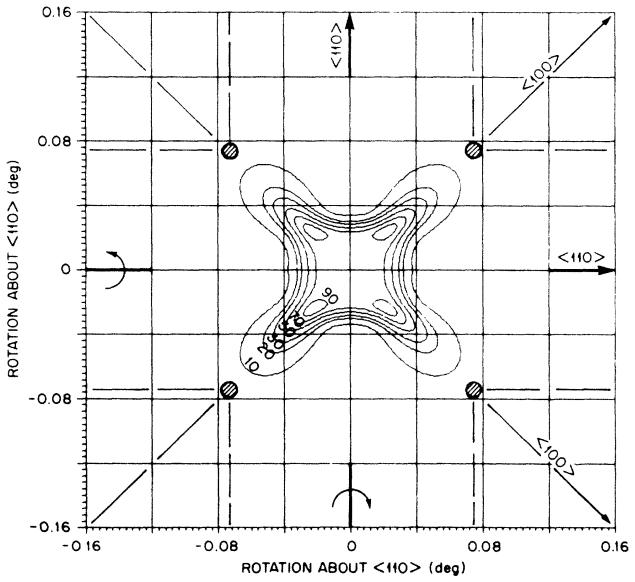

FIG. 7. The calculated angular distribution for 7-MeV protons axially channeled in the ⟨100⟩ direction of silicon. The Monte Carlo calculation assumed the Lindhard potential ($C=4.0$), measured angular resolution functions appropriate to the experiment [0.010° vertical; 0.015° horizontal (FWHM)], and the experimental crystal thickness. Cuts through the intensity distribution at a fraction of the peak intensity (percentage) are plotted as contours at the same levels as Fig. 6. The ⟨100⟩ and ⟨110⟩ axial directions are identified.

C. Monte Carlo trajectory calculations

In the Monte Carlo simulations, each projectile entered the axial channel at a randomly selected location traveling parallel to the axial direction (no beam divergence). The projectile energy loss was neglected in all calculations because the proton energy loss for our maximum crystal thickness is negligible compared to the incident energy. The ionic projectile interacted classically with each atomic string adjacent to the channel through a transverse electric field (averaged along the string) that was calculated starting from the Lindhard potential,[13] given in Eq. (3). This analytical approximation, which accounts for Thomas-Fermi screening, was chosen for the purpose of minimizing computation time,

$$V_i(x,y)=Z_1Z_2e^2\ln\left[\frac{Ca^2}{b_i^2}+1\right]. \tag{3}$$

In Eq. (3), $Z_1=1$ and $Z_2=14$ are the atomic numbers of the projectile and the target, respectively, e is the unit charge, a is the Thomas-Fermi screening length, $b_i^2=(x-x_i)^2+(y-y_i)^2$, x_i and y_i are the coordinates of the ith atomic string of the crystal, and C is a fitting parameter. Thermal vibration effects were simulated for each string by averaging Eq. (3) over the distribution function for atomic transverse displacements,[16] assuming that the atomic displacements along the x and y axes are small, independent, and given by the same Gaussian distribution. Under these assumptions, the thermally averaged potential energy for each atomic string is given by

$$V_i'(x,y)=V_i(x,y)+\frac{\sigma^2}{2}\left[\frac{\partial^2V_i(x,y)}{\partial x^2}+\frac{\partial^2V_i(x,y)}{\partial y^2}\right]. \tag{4}$$

In Eq. (4), σ is the one-dimensional thermal vibration rms amplitude, equal to 0.0744 Å,[17] to simulate room-temperature conditions. Equations (3) and (4), taken together, give the thermally averaged potential-energy contribution from the ith atomic string.

The transverse momentum imparted to the projectile in a binary collision with each string was assumed to occur at the string's center of mass. The net transverse momentum imparted to the projectile from all strings near the channel determined the net Cartesian deflection angles, as noted in Sec. II; the expressions for the Cartesian angles are given explicitly by

$$\theta_x=-\frac{N}{2E}\left[\sum_{i=1}^{M}\frac{\partial V_i'}{\partial x}\right],\quad \theta_y=-\frac{N}{2E}\left[\sum_{i=1}^{M}\frac{\partial V_i'}{\partial y}\right]. \tag{5}$$

In Eq. (5), N is the number of atoms per atomic string, E is the projectile energy, and M is the number of strings included for a given axial channel. Actual calculations showed that one should include all atomic strings lying within three coordination circles from the center of each axial channel, corresponding to $M=16$ and 20 for the $\langle 100 \rangle$ and $\langle 110 \rangle$ axes, respectively. The net deflection angle of each particle in the horizontal and vertical directions was graded using an angular bin size of 0.002°, somewhat smaller than our measured experimental resolution. As previously noted, these results were later averaged over the experimentally determined angular resolution functions (ignoring the impact-parameter-dependent broadening due to electron multiple scattering) before comparing the results to measurements.

The Lindhard potential parameter [Eq. (3)] that yielded the best fit to the measurements, $C=4.0$, is a reasonable value even though a value close to 3 was the preferred choice when the "doughnut" distribution was studied in thin silicon.[3] Deflection angles are proportional to the net electric field produced by the atomic strings surrounding the channel [Eq. (5)]; therefore one must select a potential parameter that yields a realistic field for the large impact parameters that map into the rainbow (distance from an atomic string greater than about 2.5 a.u.). The electron density in the center of the $\langle 110 \rangle$ silicon channel was estimated to be 0.067 electrons/Å^3.[18] This electron density is consistent with the density calculated from the Lindhard potential when $C=4.92$. This larger parameter also improves the agreement between the electric field derived from the Lindhard and Moliere potentials for impact parameters appropriate for rainbow scattering. The Lindhard parameter that yielded the best fit to our measurements, $C=4.0$, lies between the upper value of 4.92 and the lower value of 3 that was recommended from measurements of the "doughnut" distribution.

The model predicts that the rainbow angle is proportional to the factor, N/E, in Eq. (5). This prediction was verified experimentally for fixed thickness by comparing angular distribution measurements in the $\langle 110 \rangle$ direction taken at projectile energies of 3, 5, and 7 MeV. Indeed, the horizontal and vertical angular widths of the measured rainbow patterns (FWHM) were found to be inversely proportional to the projectile energy.

A sample Monte Carlo angular distribution for 7-MeV protons scattered in the $\langle 100 \rangle$ axial channel (using our experimental crystal thicknesses and smaller angular broadening to simulate electron multiple scattering) is shown in Fig. 8. At least 1×10^6 trajectories were run for a given axial channel. With the simplified formulation used, trajectories could be obtained at the rate of about 500/s on a Digital Equipment Corporation VAX11/750 computer, while including the interactions of 16 strings. The angular distribution obtained illustrates expected detailed features if the overall angular dispersion were about 0.006° (FWHM) (including broadening mechanisms that occur inside the crystal and a more ideal detector resolution). This assumed Gaussian half-width might apply if the estimate of the mean square angular deviation discussed in Sec. II were too large.

Several observations about Fig. 8 are pertinent. First, the rainbow ridge which is well removed from the undeflected beam position would be resolved at this improved angular resolution (see the two 60% contours which lie on each side of the rainbow ridge). Second, in moving from the rainbow ridge toward larger scattering angles, surfaces of the distribution are much steeper than those experimental results obtained with lower resolution (Fig. 6) but the general shape of the ridge differs little from the lowest level contours in our measurements. This observation gives us added confidence that we have observed the rainbow effect in axial channeling. Third, the details of each angular distribution sensitively depend on the assumed interaction potential. For example, the calculated angular location of the rainbow ridge is approximately proportional to the Lindhard parameter, C. Therefore, this constant behaves approximately like an angular magnification factor for the 2D rainbow pattern. Test calculations using the Molieré potential versus the Lindhard $C=4.92$ have shown additional smaller differences in the topology on and leading to the rainbow ridge. These observations suggest that measurements with improved angular dispersion conditions might provide a more stringent test of the axial-channel potential than was possible heretofore.

V. DISCUSSION

The rainbow effect discussed in this paper may have been observed previously but it was not explained. Golovchenko[2] performed a transmission measurement where well-aligned 2-MeV protons were channeled along the $\langle 110 \rangle$ axis of a silicon crystal that was 930 Å thick.

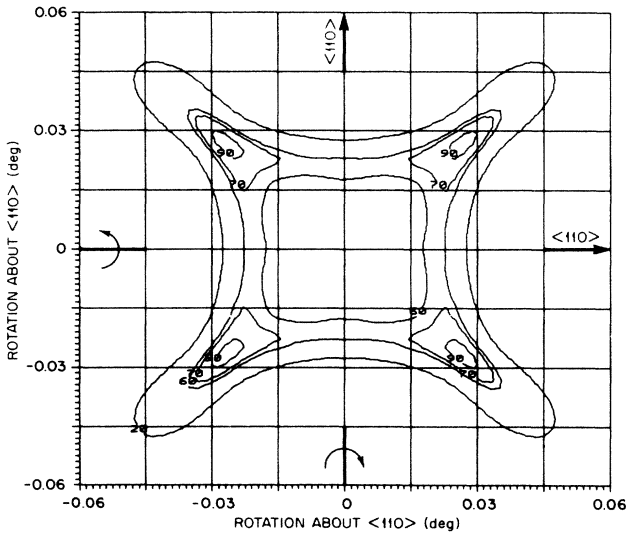

FIG. 8. A calculated angular distribution for 7-MeV protons axially channeled in the $\langle 100 \rangle$ direction of silicon which illustrates the rainbow ridge. Atomic string locations are shown in Fig. 1(a). This calculation is identical to that shown in Fig. 7 except an effective angular dispersion of 0.006° (FWHM) was used to simulate angular broadening in the crystal due to electron multiple scattering. Intensity cuts through the distribution at a fraction of the peak intensity (percentage) are plotted as contours at the 20, 60, 70, and 90 percent levels. The rainbow ridge lies between the 60 percent level contours.

The photographic record reported in his thesis was described as follows: "In the position corresponding to the initial beam direction, there appeared an intense spot with small starlike arms projecting outwards.... The symmetry of the spots is indicative of the transverse lattice of ⟨110⟩ strings.... It does not appear possible that these observations can be explained within the classical continuum picture.... It is possible that these data represent spurious results not directly caused by the interaction of the ions with the crystal."

Our classical Monte Carlo calculations performed using the proton energy and crystal thickness of Golovchenko confirm that the transverse correlation effect observed in the present investigation also should have been observable under his conditions. Although the angular size and fine details of angular distributions are sensitive to the projectile speed and the crystal thickness, the Golovchenko conditions should yield a transmission pattern that is similar to that shown in Fig. 4. This can be understood simply by scaling the angular size of the rainbow structures calculated for the present experiment to the Golovchenko conditions, using Eq. (5) that was verified experimentally. Because the projectile, the target and the channel are identical in each experiment, only the ratio of crystal thickness to projectile energy, N/E, needs to be compared in each experiment. This angular scaling factor, which describes the size of the rainbow ridge, is proportional to 1980/7 in the present case versus 930/2 for Golovchenko. Therefore, the Golovchenko angular distribution would be magnified by the factor 1.63. We ignore the bracketed summation term of Eq. (5) in this comparison because it determines the complicated mapping of an initial impact parameter into a final scattering angle for a particular projectile and geometric arrangement of atomic strings, and this mapping which is determined in a Monte Carlo calculation, is essentially identical for both experiments. Of course, some rainbow features might be modified or destroyed if increased heavy-particle multiple scattering were to occur (due to increased projectile scattering angles). This effect is not likely to have happened in the thinner Golovchenko crystal because the atomic string locations shown in Figs. 4 and 5 also would appear at amplified angular locations ($\times 1980/930$). In essence, this should lower the probability for heavy-particle multiple scattering under their experimental conditions. In conclusion, we believe that the observations of Golovchenko were not spurious results and that they are explainable within the classical continuum picture.

Although the qualitative agreement between the experimentally observed and calculated angular distributions is very good, some quantitative discrepancies were noted for both channels studied (Sec. IV). Disagreement is expected for several reasons related to the experiment. Experimental distributions cannot be normalized precisely to the angle averaged calculations because counting statistics are poorer for the experimental data. For example, fewer than 300 counts were accumulated in the ⟨110⟩ on-axis peak whereas the central peak in the simulation had more than 30 000 averaged trajectories. A comparison of experimental noise at each contour level in Fig. 4 versus that shown in Fig. 5 illustrates the statistical differences because no smoothing was performed. Imprecise normalization could have an impact on angular size of contours at any level, since all intensity cut levels are referred to the peak count. Fine structural details in the distributions could even have been missed if numerous cut levels had not been tested. Slight crystal-beam axis misalignment could contribute to observed differences. In making detailed comparisons between experiment and theory, we have previously alluded to this problem when we observed, in the case of each axis, only half the number of predicted off-axis peaks. In our visual alignment procedure, we attempted to achieve the best symmetric channeling pattern to insure that "doughnut" distributions[3] were not being measured. The degree of angular accuracy required to observe all predicted fine-structure peaks probably exceeds the capabilities of our goniometer. The misalignment issue may be resolvable using the Monte Carlo approach because it would be possible to simulate crystal misalignments and beam divergence. We recommend that future investigators construct their computer code so the effects of misalignment and beam divergence can be studied.

Disagreement between the experimental and predicted results is expected for several reasons related to our theoretical assumptions. The Monte Carlo algorithm assumed straight-line trajectories, the Lindhard continuum potential and perfect beam-crystal axis alignment, to name just a few idealizations. The assumption of straight-line trajectories overestimates the deflection for any assumed potential. This assumption is probably the principal reason that our angle-averaged Monte Carlo calculations predict the observed off-axis peaks rather precisely even though the Lindhard potential ($C=4.0$) underestimates the transverse electric field for each atomic string (Sec. IV C). This supposition was tested by comparing the impact-parameter-dependent scattering angles computed in our approximation (time-independent impact parameter involving a single string) to those numerically integrated (time-dependent impact parameter) using the same continuum potential. The result was that scattering angles determined from numerically integrated trajectores using the Lindhard $C=4.92$ agreed closely with those determined in our approximation using the Lindhard $C=4.0$ for a typical impact parameter that maps to the rainbow ridge.

Since the rainbow ridge was not resolved in our experiments with the detail illustrated in Fig. 8 for ⟨100⟩ channeling, it is appropriate to speculate about the optimum conditions for resolving it. Improved experimental design using increased distance between the crystal and the detector and improved detector spatial resolution can greatly decrease the compromised conditions of the present experiments, but we expect the effects of multiple-electron scattering to plague future experiments assuming that the Lindhard estimate noted in Sec. II is not a gross overestimate of the mean-square angular fluctuation. We believe that future investigators should adjust experimental conditions to maximize the ratio of the rainbow angle, θ_r, to the Gaussian angular width for multiple scattering. We have indicated previously that the rainbow angle scales as NZ_1/E, and does not depend on Z_2 in a significant way.

If the mean-square fluctuation for multiple-scattering scales like the Lindhard formula, ignoring the absolute magnitude, we believe it is appropriate to maximize the resolution factor given by

$$\frac{\theta_r}{[(\delta\Omega_e)^2]^{1/2}} \propto \frac{\sqrt{N}}{(\rho_e^{1/2})[\ln(4m_eE/m_1I_0Z_2)]} . \quad (6)$$

The weak dependence on crystal thickness (proportional to $\sqrt{N}$) and electron density (proportional to $\rho_e^{-1/2}$) suggests that a "thicker very thin crystal" and open axial channels are slightly more appropriate. Also, E/m_1Z_2 should be minimized. The use of a lower-velocity projectile with a quality thin crystal having a higher atomic number (e.g., germanium) should increase the probability of resolving the rainbow ridge. We discourage significant lowering of velocity, however. Our lower velocity studies, involving protons channeled in silicon at 3 and 5 MeV, increased the size of the channeling angular distribution as predicted overall, but the channeling patterns were in greater disagreement with trajectory calculations at these energies. (Disagreement at the low energies can be partially attributed to increased inaccuracies of our model and the difficulty of achieving excellent beam-crystal alignment.) Rainbow scattering investigations involving heavier projectiles (at velocities at or below what we used) also would offer the opportunity of varying the incident charge state and perhaps allow improved impact-parameter-dependent charge-changing studies to be performed in channeling.

In spite of some differences between the measured and calculated distributions, that can be partially attributed to experimental defects and pragmatic theoretical neglect, we have established the connections between the unusual focal properties of very thin crystals and individual particle trajectories. The unusual channeling patterns observed by us and others, which depend on the geometrical locations of atomic strings in a given channel, are explained by the rainbow effect. We hope that the low angular dispersion Monte Carlo calculations (Fig. 8) will challenge channeling enthusiasts to perform better experiments because a wealth of information about the scattering potential may be extractable by studying structures lying on the rainbow ridge.

VI. CONCLUSIONS

The measured angular distributions for the ⟨110⟩ and ⟨100⟩ axial channels (Figs. 4 and 6) are in excellent agreement with the averaged binary collision simulations calculated at an energy of 7 MeV (Figs. 5 and 7). Monte Carlo results obtained with small angular dispersion (0.006°) show a well-resolved ridge (maximum) whose shape is similar to the 20% contours shown in Figs. 4 and 6. Some off-axis structures in the angular distributions predicted for ⟨100⟩ and ⟨110⟩ axial channeling also have been observed at the correct angular locations. These observed structures are a part of the rainbow ridge that could not be resolved under our limited angular resolution conditions. The ridge has been shown to be the consequence of rainbow scattering within a very thin crystal by analytical and numerical investigations of the Jacobian[6] and by studying the deflection function (Sec. II). From the close correspondence between measurement and theory in both axial channels, we conclude that we have observed rainbow scattering inside a very thin crystal.

ACKNOWLEDGMENTS

The authors wish to thank Dr. Nathan Cheung of Lawrence Berkeley Laboratory for providing the silicon crystal used in these experiments. We wish to acknowledge also very helpful discussions with O. H. Crawford, and discussions with J. H. Barrett and O. S. Oen about the manuscript. This research was sponsored by the U.S. Department of Energy (Office of Basic Energy Sciences) Under Contract No. DE-AC05-84OR21400 with Martin Marietta Energy Systems, Inc.

*Present address: Boris Kidric Institute of Nuclear Sciences, 11001 Belgrade, Yugoslavia.

[1]D. S. Gemmel, Rev. Mod. Phys. **48**, 129 (1974), and references therein.

[2]J. A. Golovchenko, Ph.D. thesis, Rensselaer Polytechnic Institute, 1972 (unpublished).

[3]J. S. Rosner, W. M. Gibson, J. A. Golovchenko, A. N. Goland, and H. E. Wegner, Phys. Rev. B **18**, 1066 (1978).

[4]C. D. Moak, S. Datz, O. H. Crawford, H. F. Krause, P. F. Dittner, J. Gomez del Campo, J. A. Biggerstaff, P. D. Miller, P. Hvelplund, and H. Knudsen, Phys. Rev. A **19**, 977 (1979).

[5]N. Nesković, ORNL Report No. 60041, pp. 203–206 (1983) (unpublished).

[6]N. Nesković preceding paper, Phys. Rev. B **33**, 6030 (1986).

[7]R. Schinke and J. M. Bowman, in *Molecular Collision Dynamics*, edited by J. M. Bowman (Springer-Verlag, Berlin, 1983), pp. 61–115.

[8]A. D. Tenner, K. T. Gillen, T. C. M. Horn, J. Los, and A. W. Kleyn, Phys. Rev. Lett. **52**, 2183 (1984) and references contained therein.

[9]M. Buenard, P. Martin, R. Bertholet, C. Guet, M. Maurel, J. Mougey, H. Nifenecker, J. Pinston, P. Perrin, F. Schussler, J. Julian, J. P. Bondorf, L. Carlen, P. Kristiansson, O. B. Nielsen, A. Oskarsson, I. Otterlund, H. Ryde, B. Schroeder, and G. Tibell, Phys. Rev. C **26**, 1299 (1982).

[10]O. S. Oen, Phys. Lett. **19**, 358 (1965).

[11]Y. N. Demkov, Zh. Eksp. Teor. Fiz. **80**, 127 (1981) [Sov. Phys.—JETP **53**, 63 (1981)].

[12]See, for example, M. T. Robinson, in *Topics In Applied Physics: Sputtering by Particle Bombardment* (Springer-Verlag, Berlin, 1981).

[13]J. Lindhard, Mat. Fys. Medd. Dan. Selsk. **34**, No. 14 (1965).

[14]J. Lindhard and A. Winther, Mat. Fys. Medd. Dan. Vid. Selsk. **34**, No. 4 (1964).

[15]J. Gomez del Camp, D. Shapira, J. A. Biggerstaff, C. D. Moak, P. D. Miller, N. Nešković, R. W. Fearick, and J. P. F. Sellschop, Phys. Rev. Lett. **51**, 451 (1983).

[16]B. R. Appleton, C. Erginsoy, and W. M. Gibson, Phys. Rev. **161**, 330 (1967).

[17]B. W. Batterman and D. R. Chipman, Phys. Rev. **127**, 690 (1962).

[18]J. A. Golovchenko, A. N. Goland, J. S. Rosner, C. E. Thorn, H. E. Wegner, H. Knudsen, and C. D. Moak, Phys. Rev. B **23**, 957 (1981).